Modulation of storm-time mid-latitude ionosphere by magnetosphere-ionosphere coupling

Sebastijan Mrak[1], Joshua Semeter[1], Yukitoshi Nishimura[1], J. C. Foster[2], Marc R. Hairston[3], W. A. Bristow[4]

[1]Department of Electrical and Computer Engineering and Center for Space Physics, Boston University, Boston, MA, USA
[2]Haystack Observatory, Massachusetts Institute of Technology, Westford, MA, USA
[3]Center for Space Sciences, University of Texas at Dallas, Richardson, TX, USA
[4]Geophysical Institute, University of Alaska Fairbanks, Fairbanks, Alaska, USA

Key Points:

- We characterize mid-latitude plasma density striations (MDS) using ground-based and in-situ observations.
- The MDS are magnetically conjugate within L$\leq$2.3, with distinctive flow channels, and elevated plasma temperature.
- We find that one of the electric field excursions along the MDS resided within the ring current pressure gradient.

Corresponding author: Sebastijan Mrak, smrak@bu.edu

Abstract

We describe mid-latitude plasma density striations (MDS) modulating the evening side of Storm Enhanced Density (SED) by magnetosphere-ionosphere coupling. The MDS are magnetically conjugate, and they consist of elongated density structures [enhancements (plumes) and depletions (troughs)] that extend from the equator to the main trough equatorward boundary. Each density perturbation is associated with a flow channel, and they develop progressively at all latitudes. We present a detailed analysis of the MDS during the 7-8 September 2017 storm, by virtue of remote and in-situ observations of the magnetosphere-ionosphere system. We find that the density plumes are a result of local plasma uplift, and poleward and westward plasma transport guided by the adjacent flow channels. While the MDS's troughs bear some resemblance to the depletion patterns associated with equatorial plasma bubbles, it has been found to be quite distinct, both in terms of its observational manifestations and its formation mechanism. Namely, the trough is associated with enhanced flow channels peaking at the edges, with elevated electron and ion temperatures. Crucial spacecraft measurements of plasma parameters in the ionosphere and plasmasphere near the equatorial plane ($L \approx 1.9$) unambiguously show conjugate nature of the MDS. In particular, the magnetospheric electric field intensifications lie just earthward of the injected <200 keV ions at the ion pressure gradient.

Plain Language Summary

Geomagnetic storms are characterized by enhanced ring current, which is an electrical generator that drives enhanced sub-auroral flow in the ionosphere. A prominent consequence is an ionospheric density trough at mid-latitudes in the dusk local time sector. The location of this mid-latitude trough depends on the strength and location of the ring current injections. The trough is an important space weather threat as it facilitates plasma turbulence and it creates steep density gradients. We analyze the electrodynamic of an event, where there were multiple troughs and plasma adjacent enhancements. These mid-latitude density striations were associated with fluctuations in the electric field and convection. We show that the modulation of the electric field is field-aligned, and located earthward of the ring current. We argue the source of the modulation is a competition between electrodynamics carried by subsequent substorm injections, and impulsive enhancement of penetration electric field impacting the low-latitude ionosphere.

1 Introduction

Structured plasma depletions at mid-latitudes have been observed during geomagnetic storms (Greenspan et al., 1991; J. C. Foster & Rich, 1998; C.-s. Huang et al., 2007; Aa et al., 2019; Ma & Maruyama, 2006; Martinis et al., 2015; Zakharenkova & Cherniak, 2020) and attributed to the extreme expansion of equatorial plasma bubbles (EPB). Benchmarks for such an event were set by ground-based observations of the EPB's spatiotemporal evolution (i.e. Ma & Maruyama, 2006; Martinis et al., 2015), showing poleward expansion with a characteristic breakup at the poleward edges. The earlier in-situ observations of deep and highly structured depletions, however, were lacking spatiotemporal context (e.g. Greenspan et al., 1991; J. C. Foster & Rich, 1998; C.-s. Huang et al., 2007). Nevertheless, all events were attributed to EPBs, based on the character of in-situ plasma density depletion with embedded irregularities. The geolocation and timing were discussed in association with sunset conductivity gradients, and the vicinity of the South Atlantic Anomaly (SAA). It was Lin et al. (2007) who has sketched the geomagnetic and local time dependence. Furthermore, they found that the density depletions are paired with eastward-adjacent density enhancement. They termed these features magnetic anomaly density structures (MADS).

We build upon recent observations of mid-latitude density perturbations, during the 7-8 September 2017 geomagnetic storm (Aa et al., 2019; Zakharenkova & Cherniak, 2020). We put the observations in a context of historical literature – specifically, we bolster the conclusions of Lin et al. (2007), expand their analysis through the use of 2D total electron content (TEC) maps and conjugate in-situ observations in the ionosphere and magnetosphere. It is important to emphasize that historical observations were made during "superstorms", whereas the presented storm was associated with a maximum ring current excursion (SYM/H index) of ∼-150 nT, and at solar minimum. Nevertheless, the storm caused a sequence of episodic space weather effects, ranging from strong Ground Induced Currents in Scandinavia (Dimmock et al., 2019; Piersanti et al., 2019), Global Navigation Satellite Systems (GNSS) disruptions (Berdermann et al., 2018), extreme plasmasphere erosion (Obana et al., 2019), and a plethora of ionospheric phenomena (Aa et al., 2018, 2019).

A typical picture of the storm-time mid-latitude ionosphere at dusk consists of enhanced plasma density transported from lower latitudes (the Storm Enhanced Density - SED) (J. C. Foster, 1993), which is swept sunward by the Sub-Auroral Polarization Stream (SAPS) (J. C. Foster & Vo, 2002; J. C. Foster et al., 2007). The process of plasma redistribution is magnetically conjugate (J. C. Foster & Coster, 2007), predominantly driven by the penetration electric field (Kelley et al., 1979; J. C. Foster & Rich, 1998), and leaves a void in night-time equatorial region (Immel et al., 2005). The mid-latitude trough on the poleward boundary of the SED is a consequence of enhanced recombination (Schunk et al., 1976) driven by magnetosphere-ionosphere coupling processes (P. C. Anderson et al., 1991, 1993; Goldstein et al., 2005; E. Mishin et al., 2017).

The present study builds upon this picture by showing additional features in the (predominantly) mid-latitude ionosphere produced by a series of impulsive electrodynamic events. Specifically, we present detailed observations of SED segmentation on the evening side by enhanced plasma flows. The segmentation is morphologically similar to the plasma density striations observed by Lin et al. (2007). However, our analysis shows that the resulting density perturbations extend up to the mid-latitude trough at the poleward end. Hence, we termed the density striations as mid-latitude density striations (MDS), as the density perturbation is the most pronounced consequence. The detailed TEC maps were augmented by several fortuitous spacecraft flybys in the ionosphere and magnetosphere. The magnetospheric measurements show that one of the episodic electric field excursions, seen as a meridional flow channel in the ionosphere, resided within the ring current ion pressure gradient, just earthward of the injected <200 keV ions.

2 Observations

Solar wind parameters and geomagnetic indices for the 7-8 September 2017 geomagnetic storm are shown in Figure 1. The first three panels show Interplanetary Magnetic Field (IMF) components, solar wind speed and pressure, and geomagnetic indices for a period of ±36 hours around the storm onset. The storm commencement coincided with an arrival of an interplanetary shock (event (0)) preceding the arrival of a coronal mass ejection with increased solar wind speed ∼700 km/s. The solar wind data was taken from the OmniWeb database. The shock arrived at 23:10 Universal Time (UT) on September 7, while abruptly increased negative B_Z (<-30 nT) at 23:20 UT marks the start of the sharpest drop in SYM/H, that is the beginning of the storm main phase (event (1)). The ring current development was extremely rapid, as SYM/H decreased from -20 to -100 nT in about 10 minutes. SYM/H reached -150 nT about an hour later. Meanwhile, two episodic auroral electrojet intensifications with a strength of AL∼2000 nT (AL, shown in Figure 1f), events (2) and (3): first at 23:45 UT, and the second at 00:20 UT on September 8th. K_p index reached the value of 8 during the storm main phase. The storm (ring current) recovery began at ∼01:10 UT.

2.1 Ground-based: Ionosphere

2.1.1 Storm-time TEC evolution

We begin the analysis at around 22:00 UT on September 7, about an hour before the shock's arrival. We focus on the spatial development of ionospheric TEC over the American longitude sector and its relationship with high latitude convection. We utilized the Super Dual Auroral Radar Network (SuperDARN) from North America to compile high-resolution, local divergence-free maps of F-region $\mathbf{E}\times\mathbf{B}$ convection (Bristow et al., 2016). Figure 2 shows the spatiotemporal development of the high latitude convection (top panels), and Global Positioning System (GPS) derived TEC maps at 1 hour cadence. Vertical TEC maps are obtained from the MIT Haystack automatic procedure (Rideout & Coster, 2006; Vierinen et al., 2016). Blue vectors in the SuperDARN convection mark actual back-scatter, whereas grey vectors are the divergence-free estimates.

After two hours of negative IMF B_Z, Figures 2a-b show a coherent sunward plasma flow channel between 60-70 MLAT, guiding high density plasma from mid-latitudes towards the cusp and into the polar cap. An hour later in Figure 2c, the flow channel expanded equatorward by ∼10 degrees, now with highly structured flow vectors. On the dusk side of the enhanced sunward flow channel, the mid-latitude trough $T0$ was developing. A distinct breakup $B1$ in the enhanced sunward flow developed at 18:00 MLT. Large TEC striations appear just equatorward of that flow breakup, located in the eastward (evening side) SED boundary, and are hereafter referred to as the mid-latitude density striations (MDS). The MDS in Figure 2c consists of two troughs, denoted as $T1$ and $T2$ (outlined with broken lines), and two density plumes $P1$ and $P2$, eastward adjacent to the troughs. All parts of the MDS extended meridionally toward the equator and were magnetically conjugate. However, the observations did not capture their total extent due to sparse sampling over the Atlantic.

Figure 2d shows the MDS at 1:00 UT. The $T1$ trough developed significantly in density and width, reaching a depletion level similar to the main mid-latitude trough and a highly uniform width of ∼300 km (width similar to the adjacent plume $P1$). Simultaneously, the westward adjacent plume $P1$ also increased in density, reaching the peak TEC near 40°MLAT of 30 TECu (1 TECu = 10^{16} electrons per square meter), in contrast to the trough of 3 TECu just 300 km east. The $P1 - T1$ pair was magnetically conjugate as described in detail by Aa et al. (2019). The $T1$ trough did cut across the Equatorial Ionization Anomaly (EIA), whereas the $P1$ plume appears to be a highly elongated poleward extension of the EIA with a similar TEC at ∼1 UT. At that point, the auroral oval expanded beyond the SuperDARN coverage (∼55 MLAT), hence from this point onward all the back-scatter came from the auroral region.

Another density plume $P2$, eastward adjacent to the trough $T1$ is noteworthy. The $P2$ plume was spatially spread in contrast to the very narrow plume $P1$. While a plume-trough ($P1$-$T1$) pair much resembles the Lin et al. (2007) illustration of MDS spatial position, the additional density plume ($P2$) eastward adjacent to the $T1$ is a new feature that was not reported by Lin et al. (2007), as it doesn't extend to lower latitudes. Rather it did extend westward between the two parallel troughs, likely due to the presence of the SAPS flow.

At about 2:00 UT, the MDS began to collapse, when the parallel troughs $T0$ and $T1$ converged near 18 MLT, 45 MLAT in Figure 2e. The most pronounced change in the MDS appearance was a structural deformation in the secondary trough $T1$. The secondary trough dissolved from a compact elongated density structure into density holes highlighted in the TEC maps by the white circles. Simultaneously, the westward adjacent plume $P1$ disappeared, and the MDS slowly decayed away as illustrated in panels Figure 2f-h.

2.1.2 The development of MDS

The development of the MDS is analyzed in greater detail following Figure 3. We evaluate connections between the MDS, high latitude convection, and the sunset terminator. We utilize differential TEC (ΔTEC) maps to investigate the spatiotemporal development of the density structures, independent of the background value. The ΔTEC maps were obtained by taking a difference between two consecutive TEC maps at a 5-minute resolution, $\Delta TEC_t = TEC_t - TEC_{t-5min}$. We use the differential TEC maps as a qualitative indicator of temporal increase/decrease (red/blue) in regional column plasma density. The polarization terminator (PT) J. Foster and Erickson (2013) consists of points at a given altitude (here 100 km) where the sunset terminator at either end of the magnetic field line through that point. The PT and sunset terminators at two altitudes (100 km and 300 km) are depicted in Figure 3a – middle panel. The top panels in Figure 3 consists of the SuperDARN maps overlaid on top of the TEC maps. The TEC and subsequent differential TEC maps (middle and bottom panels) have overlaid position of the PT.

At 23:00 UT, Figure 3a, the ΔTEC map shows a large region of increasing density at mid-latitudes (i.e., the SED, red), due to local plasma uplift, and transport from lower latitudes (blue) (J. C. Foster, 1993). A local, longitudinally elongated TEC decrease just poleward of the SED is clearly identified in the differential TEC map, despite this region was still in the sunlit ionosphere. This region of local TEC decrease is co-located with enhanced sunward plasma flow identified by the SuperDARN convection map. We refer to the longitudinally decreased TEC region as the mid-latitude trough. We define the border between the mid-latitude trough and the SED the trough equatorward boundary (TEB). Ten minutes later, (Figure 3b, at the time of the shock arrival (event (0)), the ΔTEC map indicates an equatorward expansion of the mid-latitude trough and marks the first appearance of the $T1$ and $T2$ troughs. At 23:30 UT, Figure 3d, ΔTEC maps, and the SuperDARN convection clearly show co-location of the breakup point $B1$, with the poleward edge of the MDS just west of 18:00 MLT.

An equatorward deflection of the otherwise sunward flow co-located with adjacent MDS lasted for more than half an hour, the time period of episodic density increase in the MDS. The ΔTEC map indicate that the MDS emerged as slightly westward-tilted meridional structures, but already present at all latitudes below 55 MLAT at 23:30 UT. The ΔTEC maps reveal the presence of the MDS before they became apparent in the TEC maps at about 23:50 UT. Interestingly the MDS cross the PT near 40 MLAT. At the 00:10 UT Figure 3h), the peak-to-trough ($P1$–$T1$) amplitude of the MDS significantly increased, reaching values of 30 – 3 TECu, respectively.

The SuperDARN backscatter-estimated flow speed before and during the MDS development (22:00 – 01:00 UT) has constantly exceeded 1000 m/s as depicted in Figure 4. The Figure depicts equatorward expansion of the flow channel in excess of 10°MLAT, as well as it shows zonally and meridionally averages flow speeds. The backscatter came from the region of increased plasma density withing the SED plume, and the region of depleted density just poleward of it. The backscatter locations with respect to the TEC structures are depicted in the top panels of Figure 3, and in the supplemental movie S1 with 2 minute resolution.

2.1.3 The equatorial electrojet

We estimate the strength of the equatorial electrojet, and consequently the strength of the penetration electric field (PEF) utilizing low latitude magnetometers. We use data from Huancayo (HUA, Peru. 1.17°MLAT) and Kourou (KOU, French Guyana. 8.62°MLAT), to estimate the strength of the equatorial electrojet, and $\mathbf{E}\times\mathbf{B}$ upward drift at the equator (D. Anderson, 2002; Kikuchi et al., 2010). The estimated strength of the electrojet-imposed magnetic field deflection is shown in Figure 5. The magnetogram indicates the

presence of a long-lasting enhanced equatorial electrojet (positive ΔH deflection), which indicates a long-lasting presence of the eastward electric field. According to statistical formulae (cf. D. Anderson, 2002), ΔH ∼100 nT corresponds roughly to plasma uplift at equator v_{up} ∼40 m/s. Four events identified by geophysical drivers are marked on the magnetogram. Two outstanding intensifications are aligned to the storm onset, labeled (1), and the second substorm injection labeled (3).

The MDS began to develop right after the storm onset (1), at the time of abruptly enhanced electrojet. The striations, however, steadily increased in amplitude in the next hour, despite a decrease in the electrojet. By the time of the next electrojet intensification at ∼00:30 UT (3), the MDS were already well developed. An eastward electric field was present at the American longitude sector until ∼4 UT, which is local midnight in Huancayo. The inferred eastward electric field was likely the driver of upward and poleward plasma transport resulting in enhanced mid-latitude plasma density basin.

2.2 In-situ: Ionosphere

The longevity of the density structures was favorable for frequent low orbiting spacecraft flybys. We utilized measurements from the Defense Meteorological Satellite Program (DMSP), to characterize the mid-latitude ionosphere in Figure 6. We exploited the magnetic conjugacy of the MDS, in that we used measurements from southern and mapped them to the northern hemisphere. We use a mapping altitude of 350 km (the altitude used in constructing the TEC maps), using the Apex model of the geomagnetic field (Emmert et al., 2010). DMSP probed the topside ionosphere at ∼860 km, measuring ion density, composition, temperature, drift, and electron temperature. Note that electron temperature from F18 is removed due to problems with the Langmuir probe. Secondly, the ion drift meter aboard F17 has baseline issues, therefore cross-track (v_y) and vertical (v_z) ion drift amplitudes are not calibrated. The measurements, however, are valid as guidance for direction and relative trend. All ion drift velocities are in the Earth's rotational frame of reference. Resolved vectors of horizontal ion drift (from ram velocity v_x, and cross-track v_y) are in geographic coordinates and plotted along the DMSP trajectories in Figures 6a-f. The region of the mid-latitude trough ($T0$) is magenta shaded, whereas the area around the MDS is shaded in green.

The first DMSP pass (D1) in Figure 6a by the F16 satellite probed the American ionosphere sector right at the time of the first impulsive drop of the SYM/H. The horizontal flow vectors indicate the presence of a strong (∼1.6 km/s) SAPS flow that peaked at the trough equatorward boundary (53°MLAT), and it penetrated down to ∼40°MLAT. The sunward flow was associated with an upflow, reaching at ∼800 m/s, and extended equatorward for ∼2°. Then, the F18 (D2) passed right through an early stage of developing MDS. Figure 6b shows an outstanding ion flow channel associated and elongated along the $P1$ plume poleward boundary, as well as flow perturbations positively correlated with the other density perturbations within the MDS. Besides, the D2 time series plot reveals a non-uniform trough $T1$. Additionally, initial perturbations in ion temperature (Ti) are measured along with the MDS which are in quadrature with the density perturbations. The background Ti withing the $P1$ plume was at about 1,200 K, whereas a subtle increase in Ti∼1,500 K was measured within density the depletions. Vertical lines in the time-series plot highlight positive correlation between density and flow, and negative correlation with Ti.

The next flybys occurred an hour after the last impulsive event (event (3)), at a time the MDS were fully developed. First, the F16 (D3) traversed over the western United States, over the region where the MDS were entrained by the SAPS and hence parallel with the mid-latitude trough ($T0$). The F16 measured unperturbed SAPS flow encompassing both the $T0$ trough and the MDS down to 40° MLAT. Vertical drift was negligible. At that time, electron density perturbations within the MDS were already highly

structured, maintaining characteristic enhancements at either side of the secondary trough $T1$. Electron temperature (Te) was profoundly increased within both troughs.

Lastly, F17 in D4 pass traversed the area around 2:30 UT, at a time the MDS where already dissipating and the secondary $T1$ trough was reforming into the density holes. Fortuitously, the F17-D4 passed across the MDS where there was substantially wider stand-off distance to the main $T0$ trough. The F17 measured horizontal ion convection reversal in the adjacent troughs. As explained above, the F17 ion drift meter was not calibrated and thus the amplitude of the flow is ambiguous. The region of the MDS was still associated with a distinct increase in the temperatures. Both Te and Ti were distinctly elevated, both near the secondary trough $T1$, and the plume $P2$ that separated both troughs.

In aggregate, the in-situ measurements show that the density plume $P1$ and the trough $T1$ are associated with flow channels, whereas no distinct ion flows were measured above the trough $T2$. The $T2$ trough was present at the very beginning of the MDS formation, identified in the ΔTEC maps, however, it could also appear as an optical feature due to density enhancement $P1$. We lack crucial in-situ measurement at the time of the initial break up, around 09/07-23:30 UT (cf. Figure 3) when its presence was very clear. A strong ion flow along the $P1$-$T1$ boundary, reversed at $\sim$2:00 UT. There is no consistent pattern in the vertical ion flow; first, there was an upflow (until D3, 01:15UT), followed by a downflow above the MDS. Temperature measurements, however, show a persuasive electron and ion temperature increase co-located with density decrease. Lastly, ion density profiles indicate an increase of small scale irregularities within the MDS over time.

2.3 In-situ: Magnetosphere

The Radiation Belt Storm Probe A (RBSP-A) crossed the American longitude sector during an inbound flight during the MDS developing phase. Figure 7 shows selected measurements with derived quantities. Figure 7A consists of in-situ measurements of the electric field, high-frequency radio (HFR) spectra, and ion energy flux (high and low energy). The ionospheric footprint of the RBSP-A trajectory, with a modulated electric field measurement, is depicted in Figure 7C. The upper-hybrid (f_{uh}) emission, a continuous narrow-band line in the HFR spectra, is used to find the density structure. RBSP-A was first located outside the plasmasphere until $\sim$23:30 UT. It then entered the plasmasphere. However, the plasmapause was not a single boundary, but rather the satellite encountered multiple density gradients. This is consistent with the structured density observed at the equatorward boundary of the main trough. The low-density region at $\sim$23:48 UT contains a highly fluctuating electric field, which could be the SAPS wave structure (SWS) (E. V. Mishin et al., 2003). The spacecraft then traversed the plasmaspheric signature of the MDS.

The electric field measurements come from the Electric Field and Wave (EFW) instrument (Wygant et al., 2013), which is measured in the antenna frame of reference (x', y', z'). The spin-plane components (E_y', E_z') are measured directly. The component along the antenna boresight (x') cannot be measured, but is obtained assuming zero parallel electric field. We then convert the electric field to the Solar Magnetic (SM) coordinates (x, y, z). The SM electric field components are plotted in Figure 7A1. A large double hump increase in the E_x ($\sim$-20 mV/m) was observed at 00:25 UT, L$\sim$1.9, 19:00 MLT. The negative E_x component of electric field designates eastward direction in the magnetic equatorial plane, at dusk local time sector. The resulting $\mathbf{E}\times\mathbf{B}$ drift is upward and poleward along magnetic field lines. At the same time, E_y component of the electric field, pointing duskward/outward, shows correlated but smaller enhancements causing westward tilt in the resulting $\mathbf{E}\times\mathbf{B}$ drift. Ionospheric projection of the drift is therefore poleward and westward, just as measured by the DMSP-D2 pass.

The HFR spectra show a sharp decrease (within the MDS shading) at a location between the E_x spikes. The measured positions of the MDS are marked on the HFR spectra. The upper-hybrid frequency f_{uh} changed from $\sim 10^3$ Hz to $\sim$500 Hz from density plume $P1$ to the trough $T1$. That roughly corresponds to plasma density change from 12,300 cm^{-3} to 3000 cm^{-3}. Notably, another sharp density trough was measured over the Atlantic, at L=1.5, 21 MLT (68°W, 22°N), a possible signature of another trough ($T3$).

An enhancement of $\sim$100 keV ion flux (Figure 7A3) was measured by the radiation belt storm probe ion composition experiment (RBSPICE) (Mitchell et al., 2013). The high-energy ion flux penetrated down to $L \approx 2.3$ at 18 MLT. The earthward edge of high energy ions coincided with and increase in plasma density, that correspond to the secondary plume $P1$. The fiducial blue line is the RBSPICE-derived perpendicular ion pressure ($P_\perp$), showing a continues gradient up to the edge of data collection. Notably, the first E_x intensification lies within the pressure gradient with a value $\sim$1 nPa. Lower energy (<50 keV) ion flux (Figure 7A4) from the Helium, Oxygen, Proton, and Electron (HOPE) instrument (Funsten et al., 2013) show increased >10 keV flux, continuously extending the RBSPICE measurements. In the area of the MDS, there were some periodic enhancements in the $\sim$100 eV energy range. Comparing three consecutive orbits (panel B), we identify the ion flux enhancements in the RBSPICE and HOPE data are due to ring current injections, at times of the storm main phase, and substorm injections.

Mapping the RBSP-A measurements to the ionosphere puts the magnetospheric observations into the ionospheric perspective in Figure 7C. The trajectory thickness represents the electric field magnitude, while the color indicates the strength and direction of its zonal component E_x. Big oscillations in the electric field magnitude, most likely the SWS, map poleward of the trough equatorward boundary, into the SAPS channel. There is no direct evidence showing SWS to have any connection with the MDS. The most significant observation, however, is the ionospheric location of the anomalous electric field increases near the MDS. The double-hump increase is located at the boundaries of the ionospheric secondary trough $T1$, which implies the magnetospheric in-situ plasma density fluctuations with the MDS observed in the ionosphere. The double hump electric field is located near L=1.9 (45° MLAT), with an apex height of >5700 km. Because $T1$ and the in-situ density local minimum were seen on the same L-shell, the reduced density is not localized ionospheric feature, in fact, it extends to the plasmasphere along the magnetic field line. The secondary trough $T1$ extends poleward in the ionosphere up to 51° MLAT (L=2.4) at that time, which would map to 8900 km in the equatorial plane. We treat the magnetosphere-ionosphere system as electrostatic, the ionospheric trough with associated electrodynamics span from the equatorial ionosphere up to the trough equatorward boundary at L=2.4, 19:00 MLT both in the ionosphere and magnetosphere. Just like the historical observations made by Brace et al. (1974).

Lastly, we utilize the International Geomagnetic Reference Field (IGRF)-12 geomagnetic field model (Thébault et al., 2015), and electric field mapping scaling factors (Mozer, 1970), to compute magnitudes of $\mathbf{E}\times\mathbf{B}$ drift (V'_{ExB}) from the RBSP-A at the DMSP altitude (850 km). In particular, we compare the estimated drift to the drift measured by the DMSP F18-D2, which probed the MDS 30 minutes earlier in Figure 8. The DMSP drift speed at the density enhancement ($P1$) gradient peaked at 1.6 km/s and reduced to $\sim$500 m/s in the adjacent trough ($T1$). The estimated ionospheric drift from the RBSP-A (V'_{ExB}) reached 1.3 km/s at the $P1-T1$ boundary, and 1.6 km/s at the other boundary. The V'_{ExB} within the trough was $\sim$400 m/s. Conjugate spacecraft observations directly show the electric field associated features as well as density structure maps along field lines. The RBSP observations thus support the interpretation that the electric field structure driving the flow along the MDS forms as a result of the magnetosphere-ionosphere coupling, as it resided within the earthward ring current pressure gradient

region. Hence, the resulting ionospheric trough was likely driven by transport and recombination in the ionosphere (e.g., Schunk et al., 1976).

3 Discussion

We characterize the mid-latitude density striations, discuss possible driving mechanisms, and put them in context with historical observations. Specifically, we focus on mid-latitude density plumes $P1$ and $P2$, and the secondary mid-latitude trough $T1$ separating them. The other trough, $T2$ identified in the TEC maps shows no associated flow channels in the in-situ measurements, thus we cannot link it to a geophysical source. Similarly, the trough $T3$ from the RBSP-A HFR spectra lack ionospheric measurements. Every aspect of the observed mid-latitude phenomenon is intriguing and important for the space weather, however, we focus our discussion and further analysis only to the MDS development phase, up to the point the MDS began to dissipate. The dissipation and reconfiguration of the MDS require a separate study of its own.

3.1 EPB Hypothesis

From a GPS-TEC map point of view, the MDS appear to have a base at low latitude ionosphere, and then expand poleward, as it was first suggested by Aa et al. (2019). In addition, historical in-situ observations of similar (likely identical), mid-latitude phenomenon (Brace et al., 1974; Greenspan et al., 1991; J. C. Foster & Rich, 1998; C.-s. Huang et al., 2007), were inclined towards the EPB hypothesis. However, the historical studies lacked spatial context. Our study now provided comprehensive structure and evolution of the MDS by the GPS-TEC maps, contemporary high resolution convection maps and unprecedented spacecraft conjunctions.

Let's consider the possibility of extreme EPB expansion, starting with the established spatiotemporal morphology attributed to mid-latitude EPB (i.e., Ma & Maruyama, 2006; Martinis et al., 2015). In their cases, a poleward expansion of the EPB is evident by means of airglow depletion and irregularity maps. Additionally, their signatures were progressively more structured at higher latitudes, indicative of the topside non-linear bubble decay, such as bifurcation. Irregularity maps from recent studies (Aa et al., 2019; Zakharenkova & Cherniak, 2020) show rather uniform pattern along density depletions, contrary to the expected reduction with latitude. Interestingly, the DMPS F18-D2 directly measured density perturbations about 30 minutes before ground-based measured irregularities (cf., Aa et al., 2019; Zakharenkova & Cherniak, 2020). The initial irregularities, however, became highly irregular later, just like in the historical cases (Brace et al., 1974; J. C. Foster & Rich, 1998; Greenspan et al., 1991; C.-s. Huang et al., 2007).

The MDS were associated with flow channels, which we discuss in the context of the underlying density perturbations. Elevated ion drifts have been surveyed within EPBs (i.e., C.-S. Huang et al., 2010), but with significant differences in magnitude and morphology compared with the current event. Ion drifts within an EPB peak in the center and gradually decreases toward edges. In contrast, the ion drifts measured within the MDS peak at the trough's boundary with a magnitude of $\sim$5 greater than those observed within EPB's. Observations of supersonic drifts inside EPBs (e.g., Aggson et al., 1992) were observed, however within the EPB seed at the magnetic equator. The opposite morphology in flow pattern was measured both by the DMPS and the RBSP-A, 30 minutes apart. Lastly, an electrodynamic feature of the EPB is a current system that causes magnetic field deflection δB in in-situ probes, with deflections of an order of nT (Rodríguez-Zuluaga & Stolle, 2019). The DMSP did not measure any magnetic field perturbations during the flybys over the MDS (hence, not shown here). The magnetometer onboard DMSP has a resolution of 2 nT.

3.2 Penetration Electric Field

The MDS began to emerge at the storm onset, near the PT, just east to Florida, United States. The eastward electric field at low latitudes accelerates poleward plasma transport due to combined effects of the PEF, the polarization electric field at the sunset terminator (PT effect), and the reduced magnetic field strength in the vicinity of the SAA. Further, magnetic declination imposes an additional westward component in the Atlantic longitude sector. The result is a basin of dense plasma at lower mid-latitudes, close to Florida (J. Foster & Erickson, 2013), that is magnetically conjugate (J. C. Foster et al., 2007), and leaves a void in the night time equatorial ionosphere (Immel et al., 2005). The PEF was present in the equatorial region for ∼5 hours, with two prominent intensifications. As the mid-latitude density plumes, $P1$ and $P2$ were developing during that time. The $P1$ plume was specifically dense and elongated, located near the PT. Its rapid and localized enhancement is consistent with numerous observations of extreme plasma uplift during prompt PEF intensifications (Kil et al., 2007). Conversely, the second $P2$ density plume is mysterious as it was entirely located in the nightside ionosphere. As the TEC maps showed a completely empty equatorial ionosphere in the nightside, the source of the $P2$ plume should have been poleward plasma transport from lower latitudes. The eastward directed disturbance dynamo electric field in the nightside (Blanc & Richmond, 1980) could have provided the driving electric field.

3.3 Trough Morphology

The secondary trough $T1$, on the other hand, cannot be explained by any of the ionospheric low latitude mechanism except for an EPB, and plasma downflow (measured upflow). As discussed earlier, the measured electrodynamic pattern does not agree with the EPB fundamentals. Instead, we argue that a progressive development accompanied by steep gradients is a characteristic of convection and recombination driven mid-latitude trough (e.g., Moffett & Quegan, 1983, and references therein). The convection there was driven by the imposed electric field originating at the ring current earthward boundary (Goldstein et al., 2005; Toffoletto et al., 2003), as measured by the RBSP-A. This secondary trough, just like the ordinary mid-latitude trough, was initially carved by the magnetospheric electric field, which was then maintained by the polarization electric field via the resulting conductance gradient in the ionosphere. Hence, such a trough persists for a long period of time after the initial driver dies off (Moffett & Quegan, 1983; Shinbori et al., 2018). Interestingly, the initial location of the peak ion drift was located at the trough's gradients. Nevertheless, convection-driven recombination can account for the progressive erosion observed along with the MDS. Ultimately, the recombination is faster in a region of the denser plasma, hence the faster trough depletion at lower latitudes.

The secondary trough $T1$ exhibits similar ionospheric properties (plasma density profile, temperatures, temporal evolution), but with strikingly different spatial extent. The spatial extent based on the observations was confined to the dusk-evening sector, connecting the equatorial ionosphere with high latitudes. The total spatial extent, however, cannot be unambiguously determined due to the lack of observations over the Atlantic and Pacific sectors. The secondary trough reached a width of ∼300 km (before dissipation), with a minimum TEC of ∼3 TECu, (in-situ density similar to the main trough), an electron temperature increase by a factor of 2 (with respect to the denser mid-latitude plasma) and an ion temperature increase (lagging the electron temperature increase), very similar to the observations by Brace et al. (1974). The horizontal ion drift reached values of ∼1.5 km/s (calibrated F16, and F18). The horizontal drift has a conjugate electric field intensification at the ring current pressure gradient near the equatorial plane.

3.4 Current Interpretation

While plasma enhancements appear to be a transport effect, the troughs, on the other hand, need an alternative explanation. Interestingly, the $P1$ plume started developing just west of the PT, but, it did not surf the PT, in contrast to the event studied by J. Foster and Erickson (2013). Instead, its low latitude base extended into the nightside. Additionally, the plume became highly elongated (extended poleward and westward), similar to the SED plume in the presence of the strong adjacent SAPS flow (J. C. Foster, 1993). A similar situation was measured in this event when a >1km/s flow guided a plume sunward, but with a drastically different spatial figure. While the SED plume is an ionospheric manifestation of the plasmaspheric drainage plume (Foster, J C, P.J. Erickson, A.J. Coster, J. Goldstein, 2002), the secondary plume $P1$ could as well be a manifestation of another plasmaspheric feature ("dusk horn") (cf. Goldstein et al., 2005), as we provide in-situ evidence for plasmaspheric density structures.

SuperDARN maps, as well as the RBSP-A observations, provided a global context of the system response. While the magnetospheric observations provide important insight into the MDS field-aligned characteristics, it is intriguing to observe high latitude convection distortion in sync with the mid-latitude plasma restructuring. The equatorward flow excursions measured by the SuperDARN could be coincidental, however, they persisted for more than 30 minutes in the time of the MDS development. Unfortunately, SuperDARN did not directly measure the flow within the MDS, although it did measure perturbed high-latitude convection just poleward of the MDS. Hence, the causal relationship remains ambiguous. Nevertheless, plausible speculation is that the MDS are a product of a global geospace response, due to a competition of low- and high-latitude electrodynamics. On one hand, there was a long-lasting presence of the eastward electric field at low latitudes (e.g., C.-s. Huang et al., 2005): the PEF during the storm onset and the consecutive substorm injections, and disturbance dynamo at later times – in the nightside ionosphere. Also, the magnetogram provides evidence for an abrupt PEF enhancement, similar to localized enhancements measured in-situ (Kil et al., 2007). Enhanced flow channel with a conjugate electric field enhancement did exist in the inner magnetosphere located in the vicinity of the ring current injection.

While the source of the MDS formation is still somewhat speculative, we find firm evidence that the MDS are a product of magnetosphere-ionosphere coupling by virtue of conjugate DMSP-RBSP plasma observations. It is highly unlikely for an ionospheric mechanism to produce 1.6 km/s flow at mid-latitudes, which would require an eastward electric field of $\sim$50 mV/m at DMSP heights. This electric field, ultimately, resided within the ring current pressure gradient. Supersonic flows at the DMSP altitudes were measured, but only at the equator, within the base of an EPB (i.e., Aggson et al., 1992). In contrast, we find it plausible that the MDS could arise as a consequence of modified electrodynamics associated with extreme ring current injection, but displaced to the dusk local time sector. The time scale of the modification was rapid and accompanied by rotational, and enhanced ionospheric flows measured by the SuperDARN. The distorted flow measured by the SuperDARN agrees well with a model of substorm injection modeled by Yang et al. (2012). A substorm modification of the ionospheric electrodynamics reaching equatorial regions is a well-known phenomenon (Kikuchi et al., 2010; Ebihara et al., 2014; Hashimoto et al., 2017). These studies emphasized its impacts on the modified mid-latitude electric field, as well as modulation of mid-latitude convection by vortex-like flows. Nevertheless, such extreme consequences to mid-latitude density modulation have not yet been demonstrated.

4 Conclusions

We have presented observations and analysis of the MDS, anomalous plasma density modulation of the storm enhanced density. We have characterized the density stri-

ations by virtue of remote and in-situ observations in unprecedented detail. We find that the MDS developed progressively, with seed density perturbations in place prior to the later irregularities. The development took place in the midst of successive impulsive events involving prompt PEF, and episodic auroral electrojet intensifications. We summarize the observations with a pictorial illustration in Figure 9, where we build upon the sketch of Brace et al. (1974) . The illustration consists of two projections. First, the meridional cut near 19 MLT, at 1:00 UT, illustrates the density striations within and near the plasmapause boundary. The other projection illustrates the local time radial dependence of the density striation. The MDS cut through the EIA and were wrapped around the SED at mid-latitudes. The MDS consist of a series of troughs and plumes within the plasmasphere. The illustration does not include the plausible existence of another density trough $T3$, measured by the RBSP-A. We find that the MDS are positively correlated with plasma flows. We find that the electric field peaks at density gradients, making them distinct from the main mid-latitude trough as well as the EPB. In addition, the measurements show isolated plasma temperature enhancements from the main mid-latitude trough. Lastly, the mid-latitude density striations with co-located electric field perturbations in the equatorial plane were located just earthward of the <200 keV ring current ion injection, still in the region of the ion pressure gradient.

We put the observations into the historical perspective, and discuss possible geophysical drivers. The MDS developed during the period of the enhanced eastward electric field, near the polarization terminator. However, highly localized development of density structures deviated from the ordinary. The density enhancements, specifically the plume $P1$, show a characteristic nature of poleward and westward transport guided by the adjacent flow channel. A PEF by itself cannot produce such localized density as it would imply the PEF itself had dramatic zonal structure. Therefore, we argue that another source of the electric field perturbed the dusk region of the ionosphere, which resulted as a coherent sequence of density perturbations with associated flow channels. We identified a sequence of impulsive events with characteristic electric field modifications that likely served as the source of initial flow channels. In particular, crucial in-situ observations of magnetospheric plasma indicated the location of the electric field within the ring current pressure gradient.

Acknowledgments

The study was supported by NSF-AGS 1821135, NSF-AGS-1907698, NASA-0NSSC18K0657, and AFOSR FA9559-16-1-0364 awards to Boston University. The GPS TEC data, SYM/H and Kp indices are available on http://millstonehill.haystack.mit.edu/. Solar wind data and electrojet indices were taken from https://omniweb.gsfc.nasa.gov/form/omni_min.html. DMSP and SuperDARN data are currently available at http://cedar.openmadrigal.org and http://vt.superdarn.org/.

References

Aa, E., Huang, W., Liu, S., Ridley, A., Zou, S., Shi, L., ... Wang, T. (2018, mar). Midlatitude Plasma Bubbles Over China and Adjacent Areas During a Magnetic Storm on 8 September 2017. *Space Weather*, *16*(3), 321–331. Retrieved from `http://doi.wiley.com/10.1002/2017SW001776` doi: 10.1002/2017SW001776

Aa, E., Zou, S., Ridley, A., Zhang, S., Coster, A. J., Erickson, P. J., ... Ren, J. (2019). Merging of Storm Time Midlatitude Traveling Ionospheric Disturbances and Equatorial Plasma Bubbles. *Space Weather*, *17*(2), 285–298. doi: 10.1029/2018SW002101

Aggson, T. L., Burke, W. J., Maynard, N. C., Hanson, W. B., Anderson, P. C., Slavin, J. A., ... Saba, J. L. (1992). Equatorial bubbles updrafting at supersonic speeds. *Journal of Geophysical Research*, *97*(A6), 8581. doi:

10.1029/92ja00644

Anderson, D. (2002). Estimating daytime vertical ExB drift velocities in the equatorial F-region using ground-based magnetometer observations. *Geophysical Research Letters*, *29*(12), 1596. Retrieved from http://doi.wiley.com/10.1029/2001GL014562 doi: 10.1029/2001GL014562

Anderson, P. C., Hanson, W. B., Heelis, R. A., Craven, J. D., Baker, D. N., & Frank, L. A. (1993). A proposed production model of rapid subauroral ion drifts and their relationship to substorm evolution. *Journal of Geophysical Research: Space Physics*, *98*(A4), 6069–6078. doi: 10.1029/92ja01975

Anderson, P. C., Heelis, R. A., & Hanson, W. B. (1991). The ionospheric signatures of rapid subauroral ion drifts. *Journal of Geophysical Research*, *96*(A4), 5785. doi: 10.1029/90ja02651

Berdermann, J., Kriegel, M., Banyś, D., Heymann, F., Hoque, M. M., Wilken, V., ... Jakowski, N. (2018). Ionospheric Response to the X9.3 Flare on 6 September 2017 and Its Implication for Navigation Services Over Europe. *Space Weather*, *16*(10), 1604–1615. doi: 10.1029/2018SW001933

Blanc, M., & Richmond, A. (1980). The ionospheric disturbance dynamo. *Journal of Geophysical Research*, *85*(A4), 1669. Retrieved from http://doi.wiley.com/10.1029/JA085iA04p01669 doi: 10.1029/JA085iA04p01669

Brace, L. H., Maier, E. J., Hoffman, J. H., Whitteker, J., & Shepherd, G. G. (1974, dec). Deformation of the night side plasmasphere and ionosphere during the August 1972 geomagnetic storm. *Journal of Geophysical Research*, *79*(34), 5211–5218. Retrieved from http://doi.wiley.com/10.1029/JA079i034p05211 doi: 10.1029/JA079i034p05211

Bristow, W. A., Hampton, D. L., & Otto, A. (2016, feb). Highspatialresolution velocity measurements derived using Local DivergenceFree Fitting of SuperDARN observations. *Journal of Geophysical Research: Space Physics*, *121*(2), 1349–1361. Retrieved from https://onlinelibrary.wiley.com/doi/abs/10.1002/2015JA021862 doi: 10.1002/2015JA021862

Dimmock, A. P., Rosenqvist, L., Hall, J. O., Viljanen, A., Yordanova, E., Honkonen, I., ... Sjöberg, E. C. (2019). The GIC and Geomagnetic Response Over Fennoscandia to the 78 September 2017 Geomagnetic Storm. *Space Weather*(MAY). doi: 10.1029/2018SW002132

Ebihara, Y., Tanaka, T., & Kikuchi, T. (2014, sep). Counter equatorial electrojet and overshielding after substorm onset: Global MHD simulation study. *Journal of Geophysical Research: Space Physics*, *119*(9), 7281–7296. Retrieved from http://doi.wiley.com/10.1002/2014JA020065 doi: 10.1002/2014JA020065

Emmert, J. T., Richmond, A. D., & Drob, D. P. (2010). A computationally compact representation of magnetic-apex and Quasi-Dipole coordinates with smooth base vectors. *Journal of Geophysical Research: Space Physics*, *115*(8), 1–13. doi: 10.1029/2010JA015326

Foster, J., & Erickson, P. (2013, oct). Ionospheric superstorms: Polarization terminator effects in the Atlantic sector. *Journal of Atmospheric and Solar-Terrestrial Physics*, *103*, 147–156. Retrieved from http://dx.doi.org/10.1016/j.jastp.2013.04.001https://linkinghub.elsevier.com/retrieve/pii/S1364682613001144 doi: 10.1016/j.jastp.2013.04.001

Foster, J. C. (1993, feb). Storm time plasma transport at middle and high latitudes. *Journal of Geophysical Research: Space Physics*, *98*(A2), 1675–1689. Retrieved from http://doi.wiley.com/10.1029/92JA02032 doi: 10.1029/92JA02032

Foster, J. C., & Coster, A. J. (2007). Conjugate localized enhancement of total electron content at low latitudes in the American sector. *Journal of Atmospheric and Solar-Terrestrial Physics*, *69*(10-11 SPEC. ISS.), 1241–1252. doi: 10.1016/j.jastp.2006.09.012

Foster, J. C., & Rich, F. J. (1998, nov). Prompt midlatitude electric field effects

during severe geomagnetic storms. *Journal of Geophysical Research: Space Physics*, *103*(A11), 26367–26372. Retrieved from http://doi.wiley.com/10.1029/97JA03057 doi: 10.1029/97JA03057

Foster, J. C., Rideout, W., Sandel, B., Forrester, W. T., & Rich, F. J. (2007). On the relationship of SAPS to storm-enhanced density. *Journal of Atmospheric and Solar-Terrestrial Physics*, *69*(3), 303–313. doi: 10.1016/j.jastp.2006.07.021

Foster, J. C., & Vo, H. B. (2002). Average characteristics and activity dependence of the subauroral polarization stream. *Journal of Geophysical Research: Space Physics*, *107*(A12), 1–10. doi: 10.1029/2002JA009409

Foster, J C, P.J. Erickson, A.J. Coster, J. Goldstein, F. R. (2002, jan). Ionospheric signatures of plasmaspheric tails. *Geophysical Research Letters*, *29*(13), 1623. Retrieved from http://doi.wiley.com/10.1029/2002GL015067 doi: 10.1029/2002GL015067

Funsten, H. O., Skoug, R. M., Guthrie, A. A., MacDonald, E. A., Baldonado, J. R., Harper, R. W., ... Chen, J. (2013, nov). Helium, Oxygen, Proton, and Electron (HOPE) Mass Spectrometer for the Radiation Belt Storm Probes Mission. *Space Science Reviews*, *179*(1-4), 423–484. Retrieved from http://link.springer.com/10.1007/s11214-013-9968-7 doi: 10.1007/s11214-013-9968-7

Goldstein, J., Burch, J. L., & Sandel, B. R. (2005). Magnetospheric model of subauroral polarization stream. *Journal of Geophysical Research: Space Physics*, *110*(A9), 1–10. doi: 10.1029/2005JA011135

Greenspan, M. E., Rasmussen, C. E., Burke, W. J., & Abdu, M. A. (1991, aug). Equatorial density depletions observed at 840 km during the great magnetic storm of March 1989. *Journal of Geophysical Research: Space Physics*, *96*(A8), 13931–13942. Retrieved from http://doi.wiley.com/10.1029/91JA01264 doi: 10.1029/91JA01264

Hashimoto, K. K., Kikuchi, T., Tomizawa, I., & Nagatsuma, T. (2017). Substorm Overshielding Electric Field at Low Latitude on the Nightside as Observed by the HF Doppler Sounder and Magnetometers. *Journal of Geophysical Research: Space Physics*, *122*(10), 10,851–10,863. doi: 10.1002/2017JA024329

Huang, C.-S., de La Beaujardiere, O., Pfaff, R. F., Retterer, J. M., Roddy, P. A., Hunton, D. E., ... Rich, F. J. (2010, jul). Zonal drift of plasma particles inside equatorial plasma bubbles and its relation to the zonal drift of the bubble structure. *Journal of Geophysical Research: Space Physics*, *115*(A7), 1–12. Retrieved from http://doi.wiley.com/10.1029/2010JA015324 doi: 10.1029/2010JA015324

Huang, C.-s., Foster, J. C., & Kelley, M. C. (2005). Long-duration penetration of the interplanetary electric field to the low-latitude ionosphere during the main phase of magnetic storms. *Journal of Geophysical Research*, *110*(A11), A11309. Retrieved from http://doi.wiley.com/10.1029/2005JA011202 doi: 10.1029/2005JA011202

Huang, C.-s., Foster, J. C., & Sahai, Y. (2007, may). Significant depletions of the ionospheric plasma density at middle latitudes: A possible signature of equatorial spread F bubbles near the plasmapause. *Journal of Geophysical Research: Space Physics*, *112*(A5), n/a–n/a. Retrieved from http://doi.wiley.com/10.1029/2007JA012307 doi: 10.1029/2007JA012307

Immel, T. J., Foster, J. C., Coster, A. J., Mende, S. B., & Frey, H. U. (2005). Global storm time plasma redistribution imaged from the ground and space. *Geophysical Research Letters*, *32*(3), 1–5. doi: 10.1029/2004GL021120

Kelley, M. C., Fejer, B. G., & Gonzales, C. A. (1979, apr). An explanation for anomalous equatorial ionospheric electric fields associated with a northward turning of the interplanetary magnetic field. *Geophysical Research Letters*, *6*(4), 301–304. Retrieved from http://doi.wiley.com/10.1029/

GL006i004p00301 doi: 10.1029/GL006i004p00301

Kikuchi, T., Ebihara, Y., Hashimoto, K. K., Kataoka, R., Hori, T., Watari, S., & Nishitani, N. (2010, may). Penetration of the convection and overshielding electric fields to the equatorial ionosphere during a quasiperiodic DP 2 geomagnetic fluctuation event. *Journal of Geophysical Research: Space Physics*, *115*(A5), n/a–n/a. Retrieved from http://doi.wiley.com/10.1029/2008JA013948 doi: 10.1029/2008JA013948

Kil, H., Oh, S.-J., Paxton, L. J., Zhang, Y., Su, S.-Y., & Min, K.-W. (2007, may). Spike-like change of the vertical E B drift in the equatorial region during very large geomagnetic storms. *Geophysical Research Letters*, *34*(9), 2–5. Retrieved from http://doi.wiley.com/10.1029/2007GL029277 doi: 10.1029/2007GL029277

Lin, C. S., Yeh, H. C., & Chao, C. K. (2007). On a possible relationship between density depletions in the SAA region and storm-enhanced densities in the conjugate hemisphere. *Journal of Atmospheric and Solar-Terrestrial Physics*, *69*(1-2), 151–158. doi: 10.1016/j.jastp.2006.07.013

Ma, G., & Maruyama, T. (2006). A super bubble detected by dense GPS network at east Asian longitudes. *Geophysical Research Letters*, *33*(21), 1–5. doi: 10.1029/2006GL027512

Martinis, C., Baumgardner, J., Mendillo, M., Wroten, J., Coster, A., & Paxton, L. (2015). The night when the auroral and equatorial ionospheres converged. *Journal of Geophysical Research A: Space Physics*, *120*(9), 8085–8095. doi: 10.1002/2015JA021555

Mishin, E., Nishimura, Y., & Foster, J. (2017, aug). SAPS/SAID revisited: A causal relation to the substorm current wedge. *Journal of Geophysical Research: Space Physics*, *122*(8), 8516–8535. Retrieved from http://doi.wiley.com/10.1002/2017JA024263 doi: 10.1002/2017JA024263

Mishin, E. V., Burke, W. J., Huang, C. Y., & Rich, F. J. (2003). Electromagnetic wave structures within subauroral polarization streams. *Journal of Geophysical Research: Space Physics*, *108*(A8), 1–11. doi: 10.1029/2002JA009793

Mitchell, D. G., Lanzerotti, L. J., Kim, C. K., Stokes, M., Ho, G., Cooper, S., ... Kerem, S. (2013, nov). Radiation Belt Storm Probes Ion Composition Experiment (RBSPICE). *Space Science Reviews*, *179*(1-4), 263–308. Retrieved from http://link.springer.com/10.1007/s11214-013-9965-x doi: 10.1007/s11214-013-9965-x

Moffett, R. J., & Quegan, S. (1983). The mid-latitude trough in the electron concentration of the ionospheric F-layer: a review of observations and modelling. *Journal of Atmospheric and Terrestrial Physics*, *45*(5), 315–343. doi: 10.1016/S0021-9169(83)80038-5

Mozer, F. S. (1970). Electric field mapping in the ionosphere at the equatorial plane. *Planetary and Space Science*, *18*(2), 259–263. doi: 10.1016/0032-0633(70)90161-3

Obana, Y., Maruyama, N., Shinbori, A., Hashimoto, K. K., Fedrizzi, M., Nosé, M., ... Shinohara, I. (2019). Response of the IonospherePlasmasphere Coupling to the September 2017 Storm: What Erodes the Plasmasphere so Severely? *Space Weather*(September 2017), 1–16. doi: 10.1029/2019sw002168

Piersanti, M., Di Matteo, S., Carter, B. A., Currie, J., & D'Angelo, G. (2019). Geoelectric Field Evaluation During the September 2017 Geomagnetic Storm: MA.I.GIC. Model. *Space Weather*, *17*(8), 1241–1256. doi: 10.1029/2019SW002202

Rideout, W., & Coster, A. (2006, jul). Automated GPS processing for global total electron content data. *GPS Solutions*, *10*(3), 219–228. Retrieved from http://link.springer.com/10.1007/s10291-006-0029-5http://files/269/6l6882t7t21337t7.pdf doi: 10.1007/s10291-006-0029-5

Rodríguez-Zuluaga, J., & Stolle, C. (2019). Interhemispheric field-aligned currents at

the edges of equatorial plasma depletions. *Scientific Reports*, *9*(1), 1–8. doi: 10.1038/s41598-018-37955-z

Schunk, R. W., Banks, P. M., & Raitt, W. J. (1976). Effects of Electric Fields and Other Processes Upon the Nighttime High-Latitude F Layer. *J Geophys Res*, *81*(19), 3271–3282. doi: 10.1029/JA081i019p03271

Shinbori, A., Otsuka, Y., Tsugawa, T., Nishioka, M., Kumamoto, A., Tsuchiya, F., ... Nishitani, N. (2018). Temporal and Spatial Variations of Storm Time Midlatitude Ionospheric Trough Based on Global GNSS-TEC and Arase Satellite Observations. *Geophysical Research Letters*, *45*(15), 7362–7370. doi: 10.1029/2018GL078723

Thébault, E., Finlay, C. C., Beggan, C. D., Alken, P., Aubert, J., Barrois, O., ... Zvereva, T. (2015). International geomagnetic reference field: The 12th generation international geomagnetic reference field - The twelfth generation. *Earth, Planets and Space*, *67*(1). doi: 10.1186/s40623-015-0228-9

Toffoletto, F., Sazykin, S., Spiro, R., & Wolf, R. (2003). Inner magnetospheric modeling with the rice convection model. *Space Science Reviews*, *107*(1-2), 175–196. doi: 10.1023/A:1025532008047

Vierinen, J., Coster, A. J., Rideout, W. C., Erickson, P. J., & Norberg, J. (2016). Statistical framework for estimating GNSS bias. *Atmospheric Measurement Techniques*, *9*(3), 1303–1312. doi: 10.5194/amt-9-1303-2016

Wygant, J. R., Bonnell, J. W., Goetz, K., Ergun, R. E., Mozer, F. S., Bale, S. D., ... Tao, J. B. (2013, nov). The Electric Field and Waves Instruments on the Radiation Belt Storm Probes Mission. *Space Science Reviews*, *179*(1-4), 183–220. Retrieved from `http://link.springer.com/10.1007/s11214-013-0013-7` doi: 10.1007/s11214-013-0013-7

Yang, J., Toffoletto, F. R., Wolf, R. A., Sazykin, S., Ontiveros, P. A., & Weygand, J. M. (2012, apr). Large-scale current systems and ground magnetic disturbance during deep substorm injections. *Journal of Geophysical Research: Space Physics*, *117*(A4), n/a–n/a. Retrieved from `http://doi.wiley.com/10.1029/2011JA017415` doi: 10.1029/2011JA017415

Zakharenkova, I., & Cherniak, I. (2020, feb). When Plasma Streams Tie up Equatorial Plasma Irregularities with Auroral Ones. *Space Weather*, *18*(2). Retrieved from `https://onlinelibrary.wiley.com/doi/abs/10.1029/2019SW002375` doi: 10.1029/2019SW002375

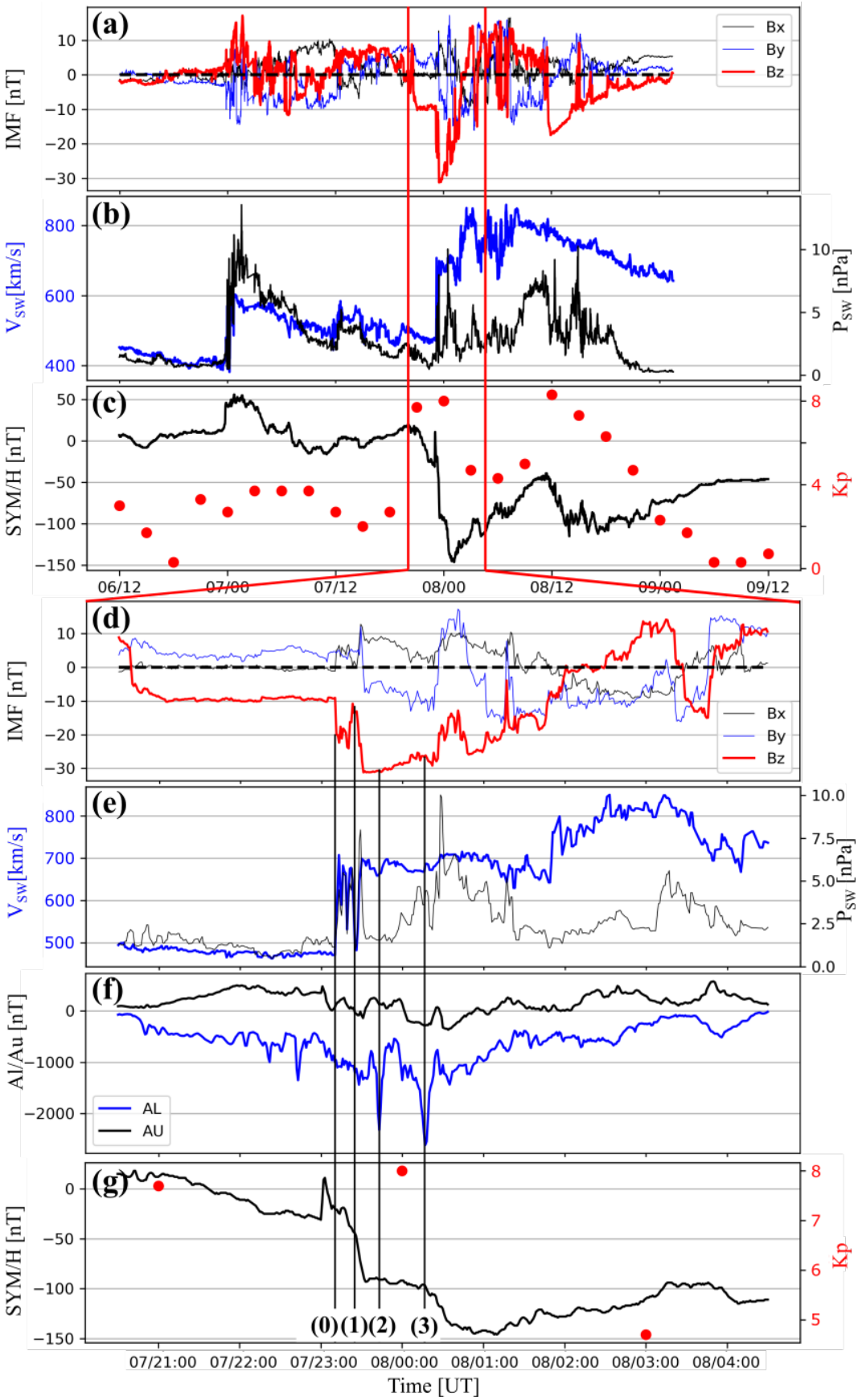

Figure 1. Solar wind and geomagnetic indices for the presented storm. (a-c) Solar wind and geomagnetic indices for a period of 3 days. (a) IMF in magnetospheric frame of reference (GSM); (b) Solar wind speed and pressure; (c) SYM/H index, and the 3-hour Kp index. (d-f) Zoomed in solar wind parameters with auroral electrojet indices for a time period of 9 hours. (d), (e), and (g) are a close up versions of upper panels; (f) Westward/Eastward (AL/AU) auroral electojet indices.

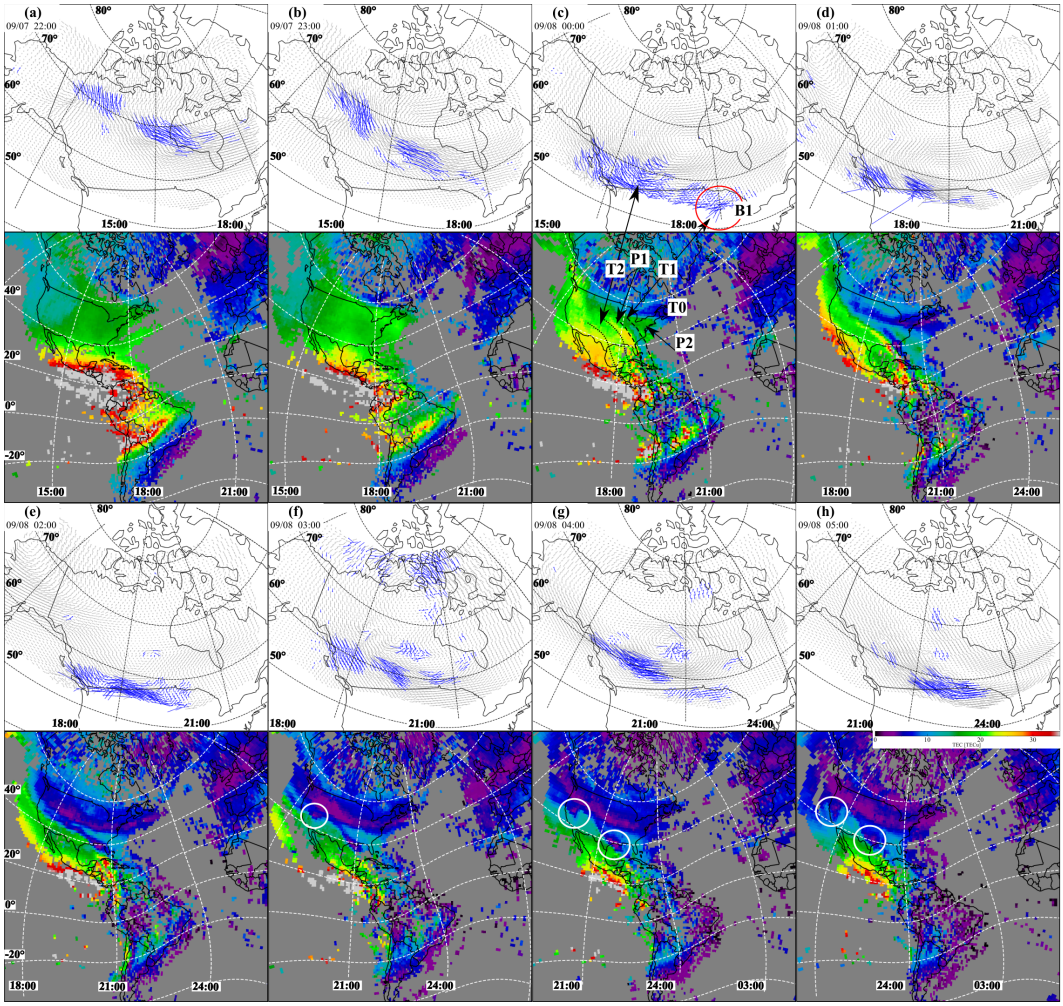

Figure 2. (a-h) Panels of high latitude convection and ionospheric TEC maps at 1 hour cadence. Each panel consists of: (top) SuperDARN convection maps using divergence-free fitting. Blue and gray vectors correspond to data points with and without radar echoes, respectively. (bottom) Global GPS TEC maps. White circles denote areas of density holes. Red circles denote location of high latitude convection breakups. Indicators are explained in text.

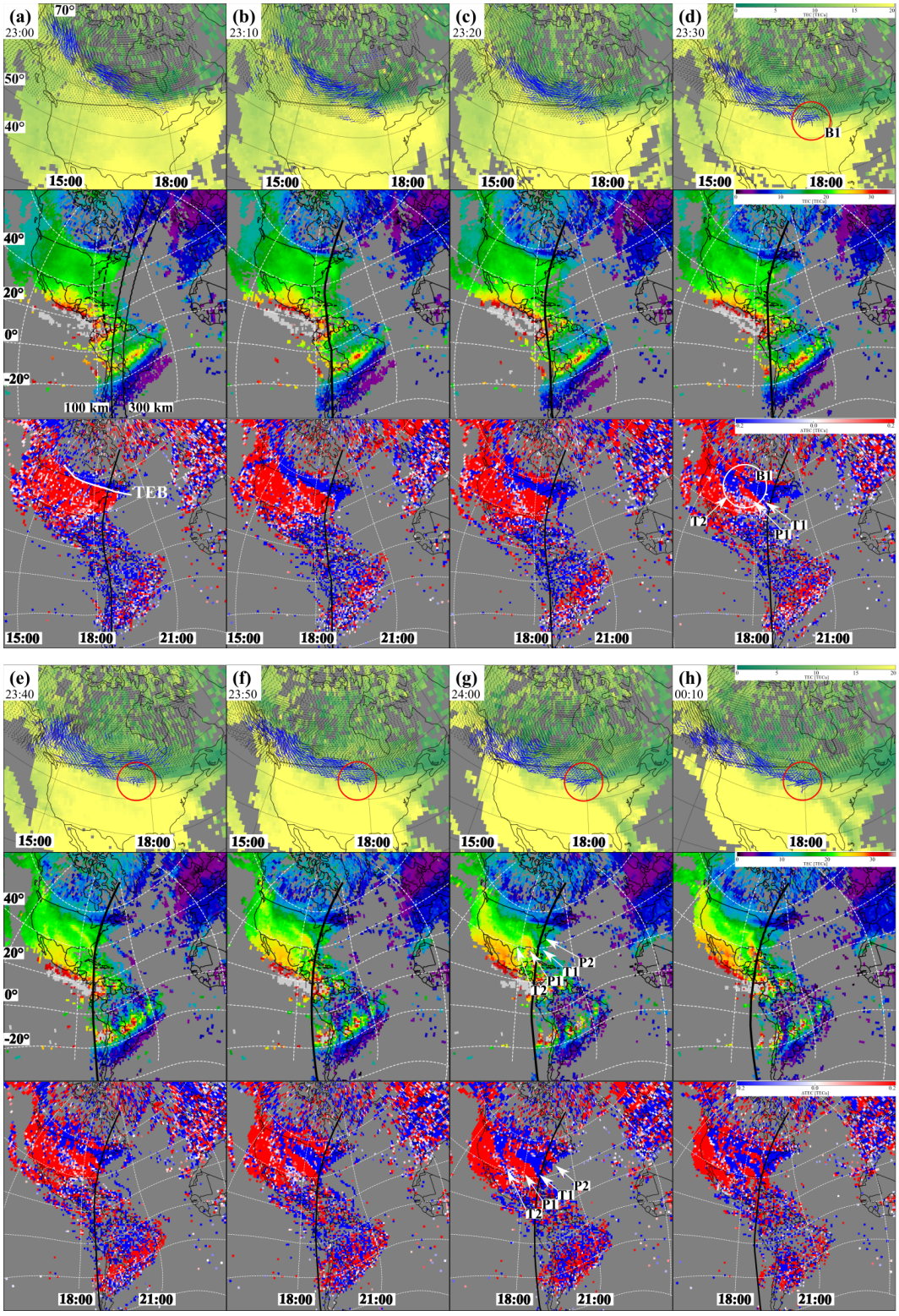

Figure 3. (a-h) Development of the MDS at 10 minute cadence. Each panel consists of: (top) SuperDARN convection on top of a GPS TEC map; (middle) GPS TEC map with a polarization terminator at 100 km. Panel (a) shows a sunset terminator at 100 km (thick) with projected conjugate terminator to northern hemisphere (dashed), and sunset terminator at 300 km (thin). Polarization terminator (PT) as defined in J. Foster and Erickson (2013) at 100 km is the bold thick in other panels; (bottom) Differential TEC maps with polarization terminator.

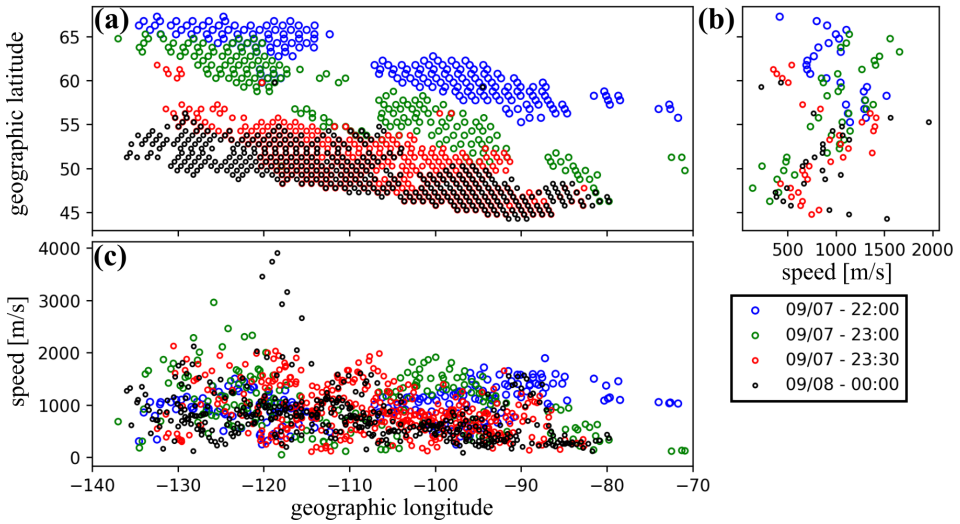

Figure 4. Backscatter-estimated SuperDARN locations and flows in geographic coordinates at four different times. (a) F-region backscatter geo-locations; (b) zonally averaged flow speed; (c) meridionally averaged flow speed.

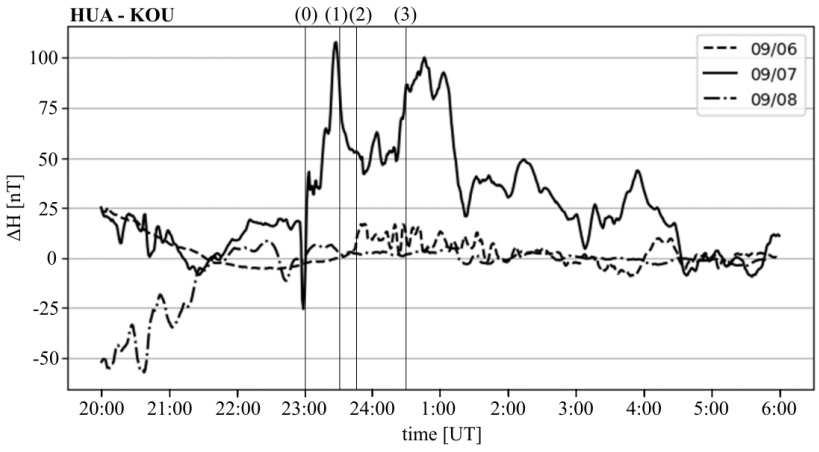

Figure 5. Equatorial electrojet measured by low latitude magnetometers from Huancayo (HUA) and Kourou (KOU) on three consecutive days at local times of the storm. Markers are defined with Figure 1.

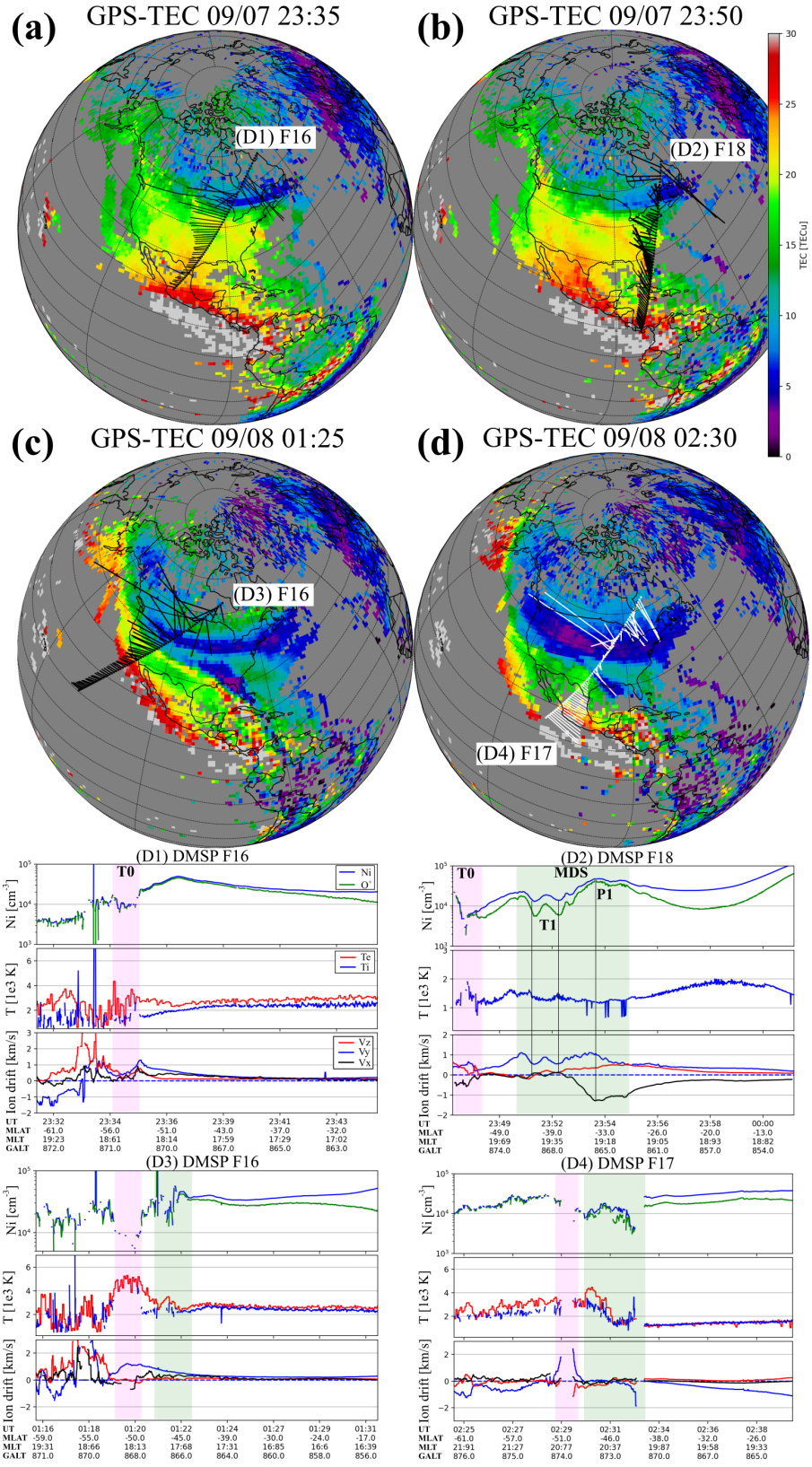

Figure 6. Ionospheric in-situ measurements of ion convection, density and temperatures. (Top panel) DMSP passes with fully resolved horizontal ion flows from selected DMSP passes (F17 vectors lengths are erroneous; see text). Trajectories are mapped to 350 km, matching the background maps of ionospheric TEC. (D1-D4) Panels show DMSP time series measurements; Density plots consist of total ion density (blue) and O^+ abundance (green), ion drift is in the Earth's rotational frame of reference. Magenta shading denote region of main min-latitude trough *T*0; green shading mark the MDS area.

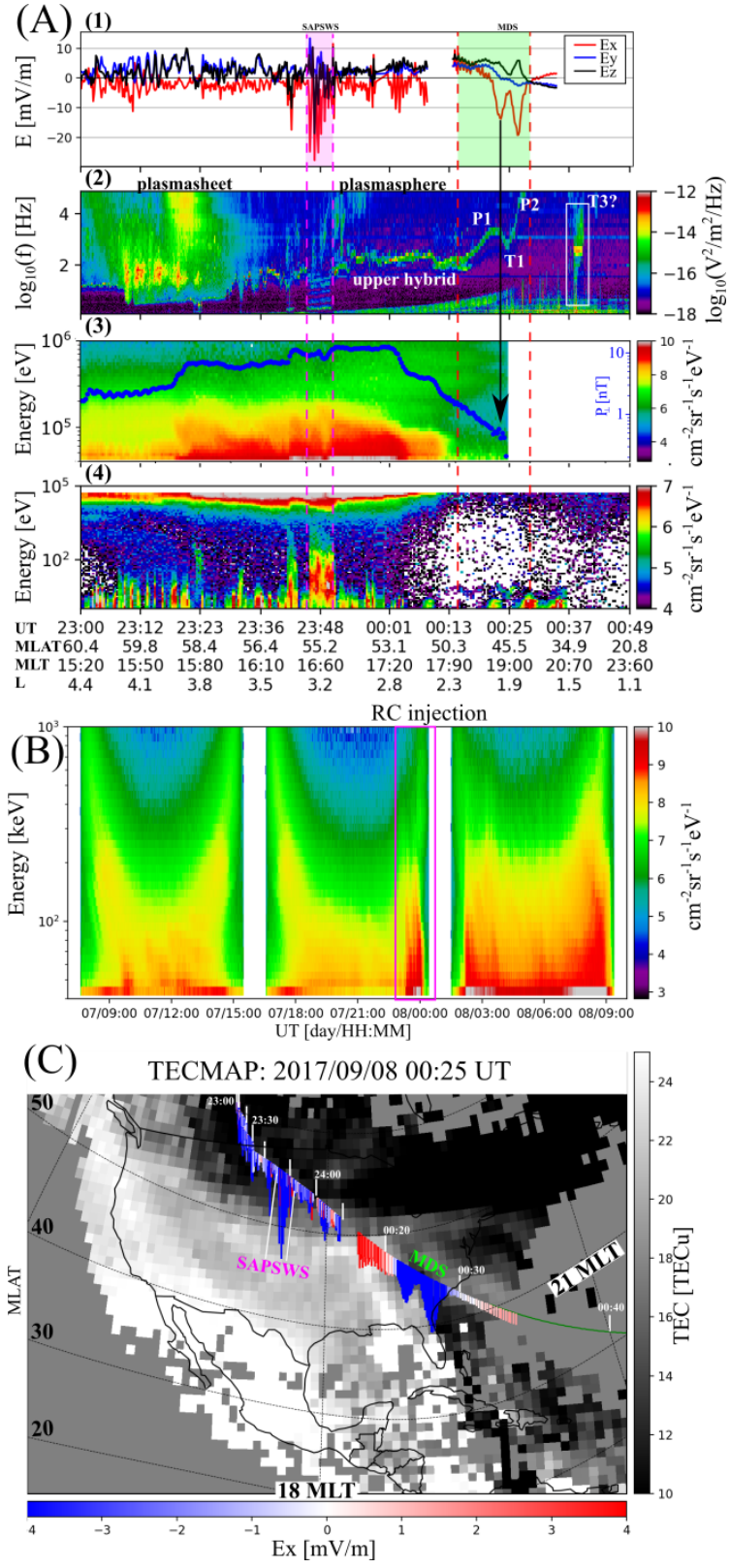

Figure 7. RBSP-A measurements and spacecraft trajectory during the conjugate observations. (A) Measurements of (1) Electric field in solar Magnetic frame of reference; (2) High frequency radio spectra from the HFR instrument, plasma frequency line is a proxy for electron density; (3) RBSPICE energy flux of high energy ions, blue fiducial line is derived perpendicular ion pressure; (4) HOPE energy flux of low energy (<50 keV) ions. (B) Three consecutive orbits of spin averaged ion flux taken by the RBSPICE instrument. The second orbit probed the dusk sector overlapping the panel (A) measurements. Indicative enhancement of <200 keV ion flux is outlined in magenta area. (C) Spacecraft trajectory mapped to northern hemisphere (350 km). Width if of the trajectory denotes electric field magnitude, color is modulated by the electric field x-component (proxy for zonal component at given local time). Markers are explained and defined in text. Background is a TEC map at 09/08-00:25 UT.

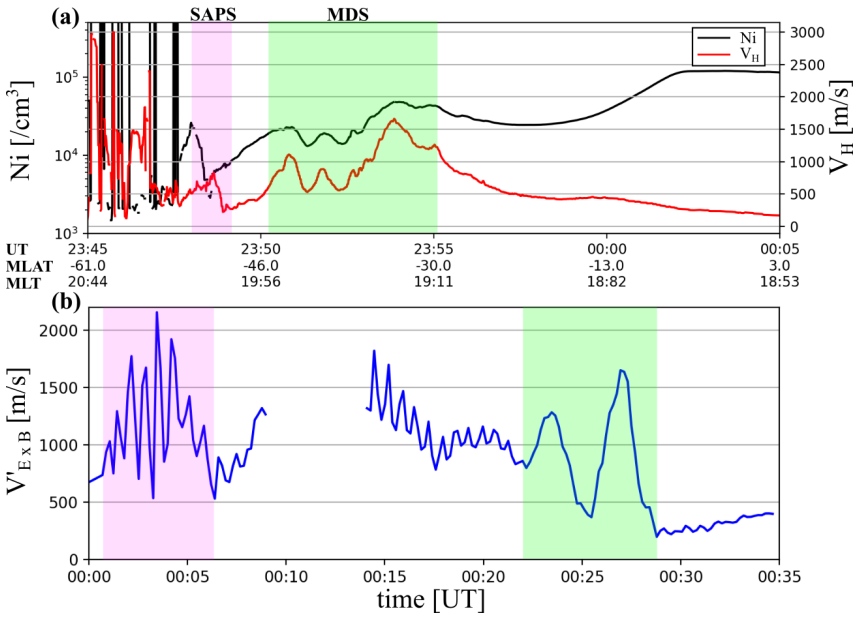

Figure 8. Direct comparison of ionospheric and magnetospheric flow speeds. (a) Measurements of the horizontal ion flow (red) and ion density (black) by the DMSP-F18. (b) Estimated ion flow magnitude at the DMSP height (850 km) by the RBSP-A measurements of electric field. The procedure is defined in text. Magenta and green shading is defined in Figure 6.

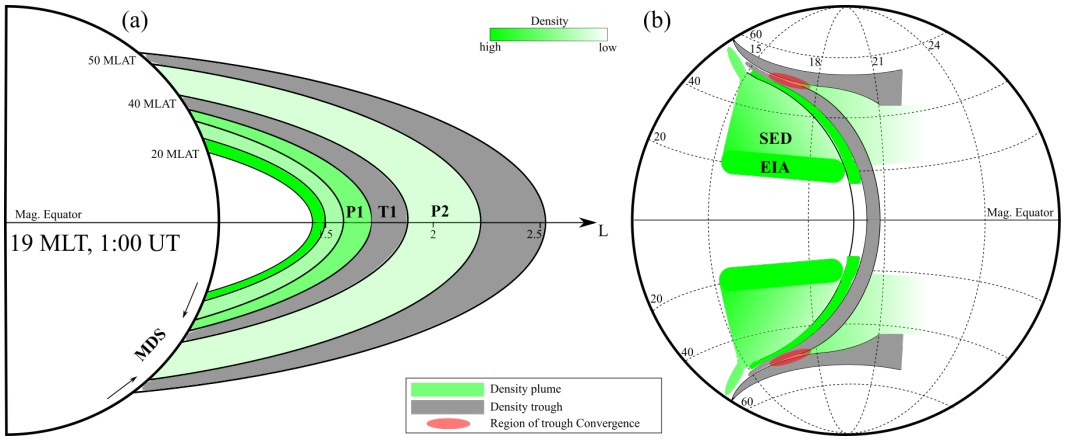

Figure 9. An illustration (not to scale!) of ionosphere-plasmasphere system configuration in geomagnetic cross-sections.